Rev. Roum. Sci. Techn.– Électrotechn. et Énerg.
Vol. **65**, *3–4*, pp. 157–164, Bucarest, 2020

NUMERICAL SIMULATION ANALYSIS OF A LINEAR MAGNETOSTRICTIVE ACTUATOR

YELDA VELI[1], ALEXANDRU-MIHAIL MOREGA[1,2], LUCIAN PÎSLARU-DĂNESCU[3], MIHAELA MOREGA[1]

***Keywords*: Magnetostriction, Magnetostrictive actuator, Terfenol-D, Pulse wide modulation (PWM) voltage excitation, PWM current excitation, Numerical simulation, Finite element.**

Magnetostrictive actuators (MSAs) are electrical machines that use magnetostrictive cores (MSC), which deform in external magnetic fields. The bias magnetic field, necessary for the proper functioning of the MSC, may be produced by permanent magnets or by electric currents. In this paper the functioning of small size, simplified, linear, MSA is analyzed using numerical simulation. A bias winding is provided to ensure the necessary pre-magnetizing state, and a drive winding, both coaxial with the MSC made of Terfenol-D. The coils are powered by PWM, power sources. Voltage and current power sources are analyzed.
The structural and electric eigenfrequencies of the MSA and its PWM source are analyzed as independent factors that concur to the electro-mechanical (displacement) of the MSA. Several conclusions, regarding the design of the MSA for optimal MSC yield are drawn.

1. INTRODUCTION

In an external magnetic field, magnetostrictive materials (MSMs) exhibit the property of deforming either by contraction or by elongation in the direction of the incident field. The MSM, which is part of the so-called "smart materials" [1–4], can be integrated with numerous devices, depending on the purpose of the application (ranging from aircraft [1], linear and rotary motors [4], vibration control [2], micro-actuation devices [5–12], and even sensors and energy harvesting devices [13–15].

The explanation for this wide range of applications that these MSMs can be integrated is given by the effect (direct, and inverse effect, respectively) exhibited by the material. The direct effect – also called the Joule effect – is characterized by the property of the MSMs to deform under the presence of the magnetic field, whilst the inverse effect – also known as the *Villari effect* – depicts the change in magnetization due to the applied mechanical stress [8].

In the case of linear MSAs, where the direct Joule effect is occurring, the mechanical deformation of the MSM drives the displacement of some specific constitutive parts of the device, *e.g.* [12], and the magnetic field required for this displacement is provided by permanent magnets [3,5,7,8,15] or by pre-magnetizing, bias currents (windings) [9,10,12].

Previous numerical studies [9,10] are concerned with small size magnetostrictive linear (displacement) motors (actuators), MSLAs, whose windings – bias and drive – are powered by current PWM (pulse width modulation) current sources of the same frequency, but with different duty cycles, *k*. The duty cycle (expressed in percentage), $k = t_{on}/T$, is defined as the "on" time, t_{on}, over the period, *T*. For exemplification purposes, Fig. 1 exemplifies a period of the PWM (here, current) supply, at f_{PWM} = 1 Hz with the duty cycle k = 30 %. Relying on the quasi (axial) symmetry of the device, the computational domains used were bidimensional. This simplification introduces some constraints associated with the drive and bias PWM power sources, because current instead of voltage (the default) may be used, which impacts the boundary conditions (BCs) that may be utilized.

This study focuses on the numerical simulation results of an MSA with a drive and a bias winding, respectively. The bias winding is sized such as to provide the right amount of prestress level necessary for optimally driving the output connector. Also, a frequency analysis is performed to establish the structural and electric eigenfrequencies that concur to an optimal magnetostrictive yield. A previous study [12] was focused on the optimal, constructal design of the magnetostrictive core, MSC, in the absence of the prestress level given by a spring. When accounted for, the spring action is modeled as a boundary condition. The spectral analysis is performed here for different prestress levels, F_{PS}, to outline its effect on the displacement of the output connector. A particular F_{PS} level is required for an optimal displacement.

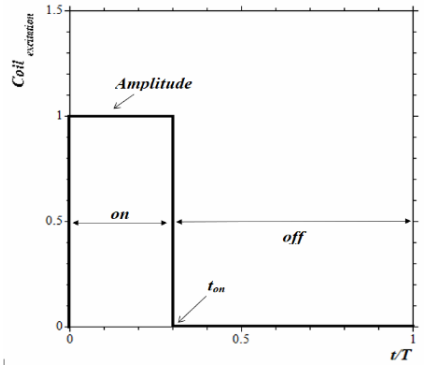

Fig. 1 – A period of a PWM signal, with a duty cycle k = 30 %.

Figure 2 presents the entire computational domain needed for the frequency analysis. The MSC made of Terfenol-D is magnetically contained in a cylindrical, accordingly sized soft iron housing. The magnetic field required for the pre-magnetization of the MSC is ensured either by permanent magnets alone or together with a magnetizing, "bias" winding [9,10,12].

A second magnetic field produced by the driving winding produces the elongation of the Terfenol-D bar that leads to the axial displacement of an output connector. Here, both the output connector and the MSC are in direct contact with an intermediate steel part, Fig. 2.

Keeping the axial-symmetry assumption for the design and the functioning, this paper extends the analysis of the MSA presented in [8,10,12] to a 3D model, which facilitates the

[1] University POLITEHNICA of Bucharest, Electrical Engineering Faculty, yelda.veli@upb.ro, amm@iem.pub.ro, mihaela@iem.pub.ro
[2] Institute of Mathematical Statistics and Applied Mathematics, Romanian Academy
[3] National Institute for Research and Development in Electrical Engineering ICPE-CA of Bucharest, lucian.pislaru@icpe-ca.ro

analysis of voltage (instead of current) PWM excitation and drive energization – a more realistic scenario.

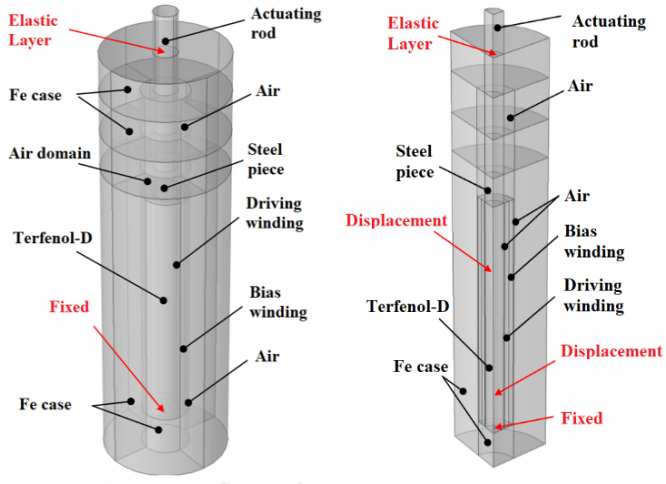

Fig. 2 – The computational domains for the MSA (left).
A quarter only (right) is needed for calculating the magnetic field.

Figure 2 presents the computational domain [12]. Whereas for the analysis of the magnetic field, by geometric and functional symmetry assumptions, the model can be reduced to just a quarter (right), for the structural, electro-mechanical problem the entire MSA (left) has to be accounted for. The structural eigenmodes of the ensemble comprise both symmetric and non-symmetric morphologies.

Numerical simulation results are presented for a small size MSA, whose drive and bias coils are both powered by PWM voltage sources, for the *on* value of 30 V.

The driving coil has 74 turns and the bias winding has 68 turns. Comparatively, the operation of this MSA is analyzed when both sources are either current or voltage sources. In both situations, the frequency of the signal (either voltage or current) is $f_{PWM} = 100$ Hz, and the duty cycle is $k = 30$ %.

2. THE MATHEMATICAL MODEL

The output connector displacement is due to the deformation of the MSC produced by the mechanical prestress and the magnetic field.

The electromagnetic field is described through Faraday, magnetic flux, Ampere, and Ohm laws, respectively [12]

$$\nabla\times\mathbf{E}=-\frac{\partial\mathbf{B}}{\partial t},\ \nabla\cdot\mathbf{B}=0,\ \nabla\times\mathbf{H}=\mathbf{J},\ \mathbf{J}=\sigma\mathbf{E}. \qquad (1)$$

Here **E** [V/m] is the electric field strength, **B** [T] the magnetic flux density, **H** [A/m] the magnetic field strength, **J** [A/m^2] the electric current density, σ [S/m] the electrical conductivity, and μ [H/m] the permeability. Because the PWM power source frequency is relatively low (≤ 100 Hz), the magnetic field produced by the displacement current is neglected in this study.

The linear forms of the magnetostrictive constitutive laws that describe the coupling inside the MSC are [16–22]

$$\begin{aligned} S &= \eta_H T + dH \\ B &= dT + \mu_T H \end{aligned}, \qquad (2)$$

where S [/] is the strain, T [N/m^2] the mechanical stress, $\eta_H = \partial S/\partial H$ is the compliance at constant magnetic strength (reciprocal of Young's modulus), d [m/A] the piezomagnetic strain constant, and μ_T [H/m] the magnetic permeability at constant stress.

The analysis is simplified here by considering that the mechanical load of the MSC and its deformation are essentially unidirectional, in axial *Oz*-direction, and gravity is neglected.

Moreover, the electromagnetic body force, **J**×**B**, produced by the induced electric currents within the MSC is neglected. The stress-strain relation due to the prestress (static load) of the MSC is described thorough the generalized Hooke's law [7,8]

$$T = C(S - S_i) + T_i, \qquad (3)$$

where C [N/m] is the stiffness, and $(\cdot)_i$ denotes the initial state. The uniaxial assumption relates the change in the shape of the MSC to the strain through $S = \partial w/\partial z$, subject to the strain gradient $\partial T/\partial z = \rho\,\partial^2 w/\partial z^2$, where $w = w(z(t))$ is the position and ρ [kg/m^3] is the mass density.

Using (1), (2), and the above uniaxial (*Oz*-direction) forms of the strain-stress and strain gradient – strain relation, yields the unsteady mathematical model for the MSC [17,23]

$$\begin{aligned} &\frac{-\rho d^2}{\mu}\frac{\partial^2 H}{\partial t^2}+\mu\sigma\frac{\partial H}{\partial t}=\nabla^2 H+\frac{d\rho\eta}{\mu}\frac{\partial^2 T}{\partial t^2}-\sigma d\frac{\partial T}{\partial t}, \\ &\rho\eta\frac{\partial^2 T}{\partial t^2}=\frac{\partial^2 T}{\partial z^2}-\rho d\frac{\partial^2 H}{\partial t^2}. \end{aligned} \qquad (4)$$

The coupling (2) holds for the MSC domain only. Elsewhere $\mu_T = \mu$ and $\mathbf{B} = \mu\mathbf{H}$, and the laws (1) then yield

$$\mu\sigma\frac{\partial\mathbf{H}}{\partial t}=\nabla^2\mathbf{H}. \qquad (5)$$

The boundary conditions for the structural mechanical problem are presented in Fig. 2, [24].

The windings are "numerical, multi-turn", made of concentric, circular turns [25]. They may be powered either voltage and, or current sources.

In this study, the loose end of the output connector does not stand any mechanical load. The base of the MSA is set fixed. The contact between the intermediate Steel piece and the upper pad of the exterior shell (Fe-case) is seen as a rod-slip fit bearing.

The mathematical model (3)–(5) was solved numerically, using the FEM technique, as implemented by [25]. First, an EMF energy equivalent PWM voltage-powering scheme is discussed. Then the mechanically unconstrained (no mechanical pres-stress) actuation is analyzed.

Progressively, the mechanical prestress (provided by a spring) required to stabilize the MSA functioning is found. The friction between the moving parts (rod and slip fit bearing) is touched too.

3. NUMERICAL SIMULATION RESULTS

3.1. THE PWM VOLTAGE EXCITATION

Symmetry may reduce the model to a bi-dimensional problem that may be used through the magneto-mechanical analysis of the MSA. However, in this simplified approach [8,11], the magnetic field source has to be a current, namely the ampere-turns of the windings. While providing useful insights into the MSA functioning, the current energizing mode is less encountered in practice where sources are more commonly of voltage type [9].

Figure 3,a shows the bias and driving ampere-turns when current PWM sources are used for both windings [11]. To

swap to a PWM voltage supply, here, the voltage is adjusted such as to keep approx. the same energizing level.

Figure 3,b shows the ampere-turns thus calculated from the output of the PWM voltage excitation model. As expected, the ampere-turns profiles are different, which cautions that the pending electro-mechanical dynamics of the MSM, basically the displacements of the connector – may be different too.

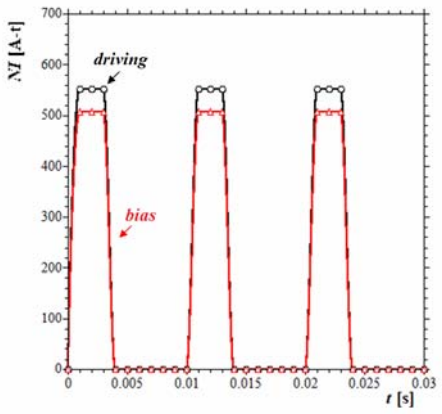

a) Current excitation is used for both windings.

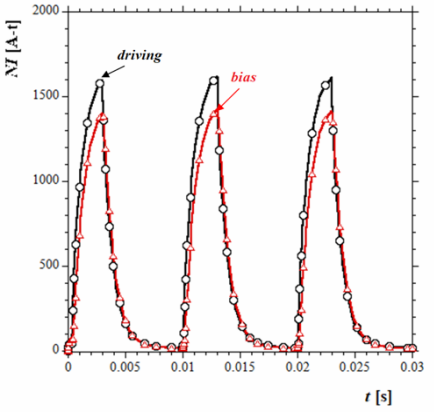

b) The ampere-turns when voltage excitation is used.

Fig. 3 – The driving and the bias ampere-turns for PWM voltage source, with $f = 100$ Hz, and $k = 30$ %, prestress $F_{PS} = 500$ N/m.

The numerical experiments presented in what follows are related mainly to a PWM voltage source, for both windings.

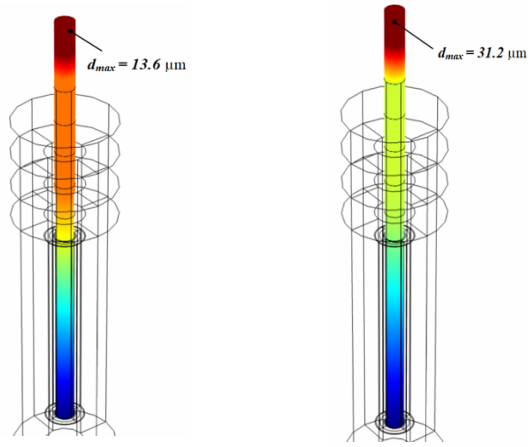

a) At $t = 0.212$ s. b) At $t = 0.032$ s.

Fig. 4 – The displacement of the output connector. Friction is neglected.

A glimpse in the deformation of the MSC structure is provided by Fig. 4, which presents the displacement (amplified 5 times) for two moments that correspond to the extreme (lower and upper) positions of the output connector, with the prestress $F_{PS} = 500$ N/m (Figs. 2,3,7).

3.2. THE MECHANICAL PRESTRESS

It has been shown that the rotation of magnetic moments under mechanical stress may have a potential role in controlling the magnetostriction yield therefore the shape anisotropy of the MSC may be adjusted and used to lead to the highest possible deformation. Whereas processing techniques, such as stress annealing and field annealing are available, mechanical prestresses may also induce alignment perpendicular to actuation if the stress is lower than the buckling limit [18]: a unidirectional (axial) compressive prestress of up to ~50 MPa can amplify magnetostriction by ~90 %. This is explained by a "jump" in the initial alignment of domains orthogonal to applied stress and the improved final alignment parallel to the applied stress.

Therefore, in this study, the MSA is provided with a spring that ensures the mechanical, uniaxial prestress of the MSC part. The sensitivity of the magnetostrictive yield concerning the mechanical prestress level, of importance in the design of the MSA, is evidenced here by numerical simulation.

Moreover, if no external means of holding the MSC are employed (for example epoxy), the MSC can push but not pull the output connector. A prestress mechanism is recommended to provide the return force needed to keep the output connector and external load moving with the MSC. This part has to be designed such as to ensure operation at sufficiently large magnetic drive levels [22]. The peak acceleration for harmonic output d_{max} of the MSC is limited then by the nominal prestress, F_{PS}, the area of the rod, A, and the effective dynamic mass M_{eff} by $d_{max} \le F_{PS} A / M_{eff}$.

Figure 5 presents the output connector displacement for PWM excitation methods, both voltage and current when friction is neglected.

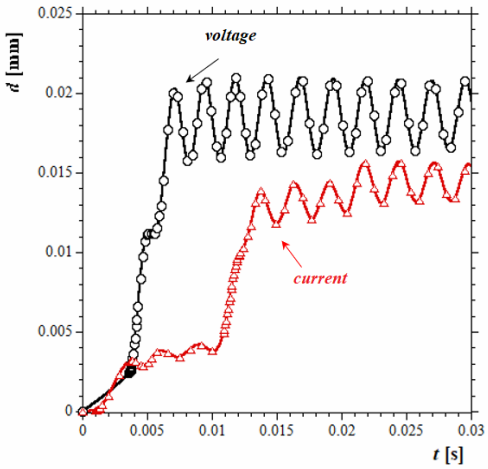

Fig. 5 – The displacement of the output connector for PWM voltage and current excitation, at $f = 100$ Hz and $k = 30$ % – without prestress. Friction is neglected.

The transient regime to quasi-steady state, when starting from homogeneous initial conditions, is shorter when voltage sources are used. The output connector maximum displacement (22 mm *vs.* 16 mm) and peak-to-peak excursion (~5.5 *vs.* ~3.5 μm) are larger when voltage control is used but increasing the current amplitude (by tuning the voltage) may compensate for it.

The output connector would not return to the rest positions, and mechanical prestress is therefore needed.

However, as friction may inevitably add to the mechanical load, its effect is next analyzed before continuing to the prestress analysis.

3.3. THE EFFECT OF FRICTION IN THE OUTPUT CONNECTOR-SLIP FIT BEARING

The frictions between the different parts that are in relative motion concerning each other are a menace for the MSA functioning. Besides the power loss, the accompanying heating may result in local expansions of the contacting, amplifying eventually the process to the limit of blocking the device.

Therefore, the MSA design has to envisage solutions to reduce as much as possible if not suppress them. In this section we touch this aspect by accounting for the friction in the rod – slip fit bearing ensemble, in the process of adjusting the prestress force required to stabilize the MSA.

The output connector displacement, with friction, c_f = 0.01 [26,27], and without friction, for voltage control, as shown in Fig. 6. Friction not only reduces the displacement amplitude and peak-to-peak excursion, but it has a damping effect too by retarding the output connector reaction time to the PWM control.

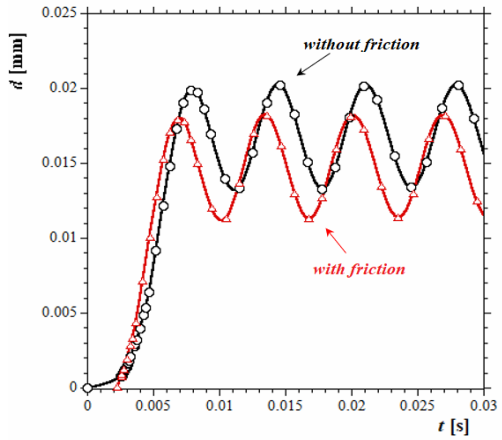

Fig. 6 – The displacement of the output connector for voltage excitation, f = 100 Hz, and k = 30 %, with (c_f = 0.01) and without friction.

Because the numerical effort (integration time) is considerably larger when friction is accounted for, *e.g.*, for aerospace applications [9], in what follows this effect is discarded. Although prone to this simplification, the results presented next to show off, qualitatively, and close enough quantitatively, features, and conclusions that can be distinguished using frictionless models too.

3.4. THE ADJUSTMENT OF THE PRESTRESS FORCE

Figure 7 reveals the phase delay between the displacements and the PWM voltage (dotted line), for different prestress levels, F_{PS}. The PWM leading signal (voltage) is also plotted, to evidence the discrepancy between the electric signals and the corresponding mechanical displacements.

As seen before, slightly larger displacements are obtained when friction is discarded, and the displacement slightly lags when friction intervenes. However, friction may have a greater impact over the heat transfer analysis, which is not addressed here though.

Interestingly enough, increasing the prestress (*e.g.*, from 500 N/m to 1200 N/m) reduces the frequency of the displacement oscillation, approaching it to the PWM frequency. Further increasing it (*e.g.*, 2355 N/m) continues this trend, but secondary frequencies (for the displacement) are seen to emerge.

These findings suggest that there should be a relation between the mechanical eigenfrequencies of the MSA and the electromagnetic properties and PWM frequency spectrum, which is discussed in the section to come. Again, friction is a factor in this shift, but the study of its impact makes the object of future work.

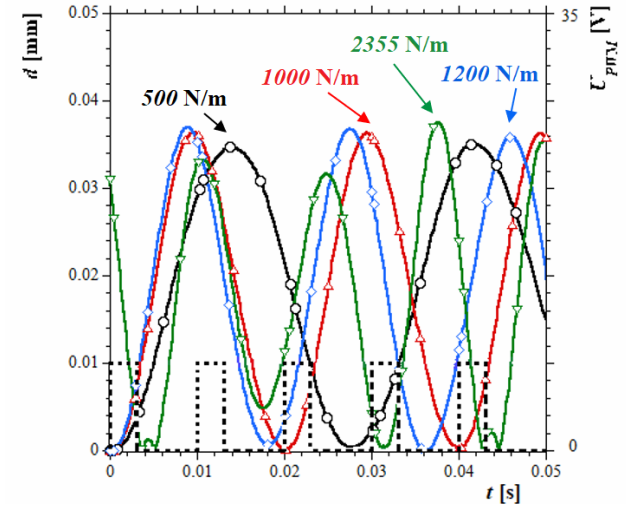

Fig. 7 – The displacement of the output connector for increasing prestress.

3.4. MECHANICAL-ELECTRIC SPECTRAL ANALYSIS

The MSA is a mechanical-electromagnetic system whose complex dynamic is controlled by its structural (mechanical) and electromagnetic dynamic properties.

The different, device-dependent time constants concur with the PWM source time constant, and their knowledge and adjustment are key factors in optimizing the MSA functioning. This section is devoted to the analysis of the mechanical eigenfrequencies and the PWM signal harmonization required for optimal functioning.

We conjecture that the fundamental frequency of the PWM signal is a key factor, which stems from the electric control. This assertion will be validated through numerical simulations. Furthermore, the prestress is another key factor, a control, of the structural part of the MSA. The electromagnetic properties of the MSA "convolve" the electric control (PWM) applied to the MSA structure, which executes the work upon the external load.

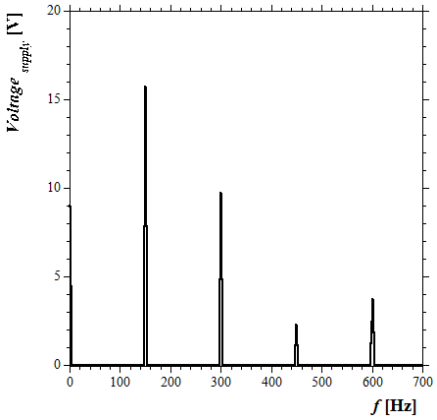

Fig. 8 – The frequency component magnitudes for PWM voltage control, at 30 V, f_{PWM} = 100 Hz, k = 30 %.

Along this path, first, the frequency spectrum of the PWM voltage supply at 30 V, f = 100 Hz, k = 30 % is

found, Fig. 8. The first, the fundamental frequency is found at f_e = 150 Hz, called in what follows "electric" frequency. This frequency and the PWM frequency (f_{PWM} = 100 Hz) will be compared with the "structural" (mechanical) eigenfrequencies, and the connector displacement ones, to probe the electro-mechanical structural behavior of the MSA, and to adjust the PWM control to ensure maximum magnetostrictive yield.

Next, the eigenmode analysis of the MSA reveals the four most important structural eigenfrequencies, f_m, found around f_e. The "structural" frequencies vary with the prestress level, as seen in Table 1.

Table 1

The structural eigenfrequencies around f_e = 150 Hz (f_{PWM} = 100 Hz) for different prestress levels, F_{PS}, without friction.

F_{PS} [N/m]	$f_{m,1}$ [Hz]	$f_{m,2}$ [Hz]	$f_{m,3}$ [Hz]	$f_{m,4}$ [Hz]
500	43.237	70.511	132.51	213.04
750	47.571	85.113	138.23	263.01
1,000	49.815	97.583	**143.84**	293.583
1,200	48.986	102.406	**158.02**	291.437
1,500	47.396	119.245	164.24	292.951
2,355	47.368	**150.001**	188.11	290.87

The numerical simulations were performed for the entire MSA (Fig. 2, left) and not just a quarter of it (Fig. 2, right) as in the electromagnetic analysis. The reason is that unsymmetrical modes and deformations may thus be evidenced. Figure 9 graphs the data in Table 1.

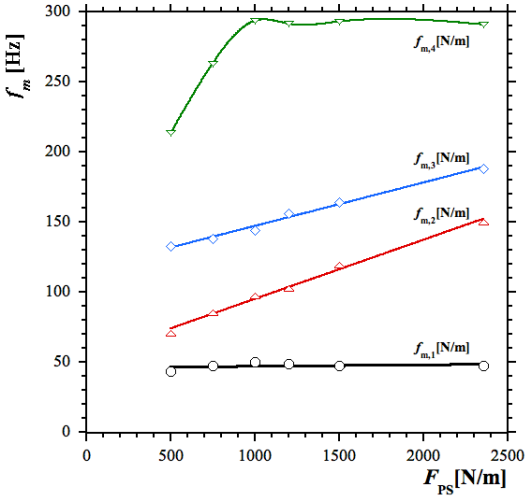

Fig. 9 – The structural eigenfrequencies for different prestress values.

It is interesting to note that, increasing F_{PS}, the first and fourth frequencies remain constant ($f_{m,1}$ for almost the entire range, whereas the $f_{m,4}$ past a region of linear increase), whereas the second and third frequencies vary linearly (within the accuracy limits of the numerical simulations) with F_{PS}. The question remains though if, for higher F_{PS}, the $f_{m,2}$, and $f_{m,3}$ curves, would depart this behavior to reach, as $f_{m,1}$, and $f_{m,4}$, a plateau (constant) value. Anyhow, because spurious oscillations occur for larger F_{PS}, this analysis seems of less concern here.

The need for increasing F_{PS} resides from the fact that for the initial prestress F_{PS} = 500 N/m, near the resonance frequency of the device, $f_{m,3}$ (the closest to f_e = 150 Hz, and not to f_{PWM}) the displacement of the output connector presents some oscillations that are likely to destabilize the system. The best tuned electric / mechanical frequencies (~150 Hz), is recorded for 2,335 N/m ($f_{m,2}$ = 150 Hz). A prestress of ~1,100 N/m would excite the $f_{m,3}$ mode. Moreover, although f_e and f_{PWM} are inevitably related, it seems that the electric rather than the PWM frequency is sometimes a more relevant and convenient design parameter.

3.5. PWM FREQUENCY TUNING

The spectrum of the PWM signal and that of the MSA structure for a specific framing and prestress, F_{PS}, are independent quantities that may concur in predicting the MSA functioning. The adjustment of the PWM voltage source frequency, f_{PWM}, should observe the structural eigenfrequencies of the MSA when aiming to enhance the displacement yield of the output connector and a more stable operating mode. Therefore, their knowledge – PWM and structural frequencies – is an initial step in the MSA tuning.

To investigate the validity of this assumption, we consider the MSA functioning for F_{PS} = 500 N/m (first line in Table 1). Table 2 lists the fundamental frequency, f_e, and the first three significant displacement frequencies, f_d, for f_{PWM} = 100 Hz, 85 Hz, and 43 Hz (30 V, k = 30%). Friction is neglected here.

Table 2

The electric, f_e, and the displacement frequencies, f_d, for different f_{PWM} *.

f_{PWM} [Hz]	f_e [Hz] **	f_d [Hz] *		
		$f_{d,1}$	$f_{d,2}$	$f_{d,3}$
43	68	7.45	9.09	1.63
85	127	5.11	7.06	17.05
100	150	8.36	3.58	20.30

* k = 30 %, F_{PS} = 500 N/m; ** Rounded off values.

Figure 10 renders the displacement of the connector for these cases. The spectral content of d is presented in Fig. 11 and the frequencies of the first three largest displacements are listed in Table 2. Increasing f_{PWM} slightly reduces the amplitude of the displacement however the spurious frequencies lose significance (*e.g.*, compare Fig. 10,a and Fig. 10,c).

Table 1 shows off a structural eigenfrequency ($f_{m,1}$ = 43.237 Hz) that is close to f_{PWM} = 43 Hz, and another one ($f_{m,2}$ = 70.511 Hz) relatively close to its associated f_e = 68 Hz, but no structural eigenfrequency is detected closer either to f_{PWM} = 85 Hz (f_e = 100 Hz) or to f_{PWM} = 100 Hz (f_e = 150 Hz).

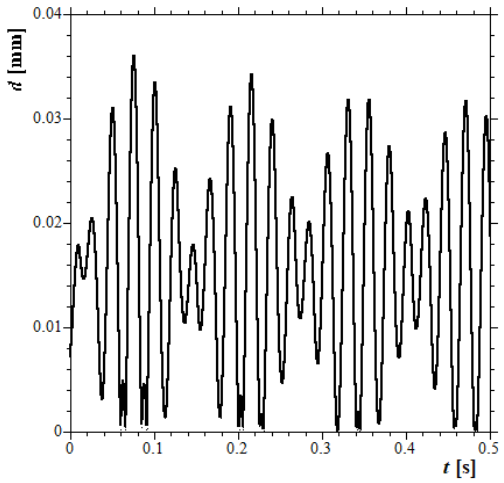

a) f_{PWM} = 43 Hz, f_e = 68 Hz.

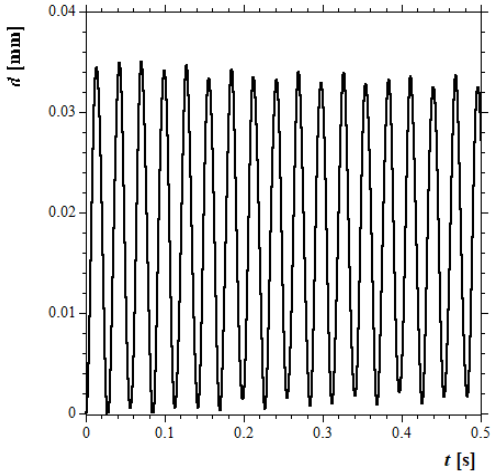

b) f_{PWM} = 85 Hz, f_e = 127 Hz.

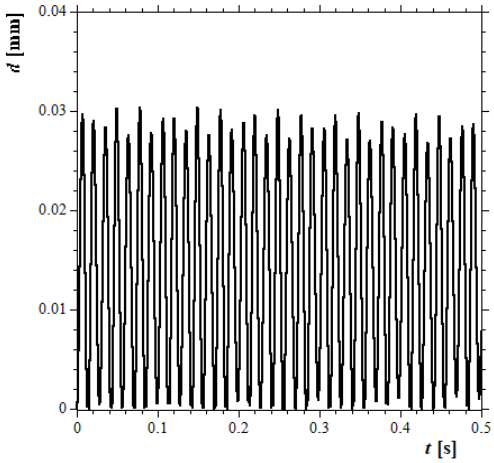

c) f_{PWM} = 100 Hz, f_e = 150 Hz.

Fig. 10 – The displacement of the output connector for different PWM frequencies and the associated electric frequencies.

The fundamental electric frequency for the PWM voltage at 43 Hz is around f_e ~ 68 Hz, which is close to the mechanical eigenfrequency $f_{m,2}$ = 70.511 Hz (first line in Table 1).

This PWM frequency seems to kindle a structural eigenfrequency resulting in an enhanced connector displacement. However, cyclic lobes with approx. 0.12 s periodicity emerge, as seen in Fig. 10,a, and this may be of concern to a stable operating mode.

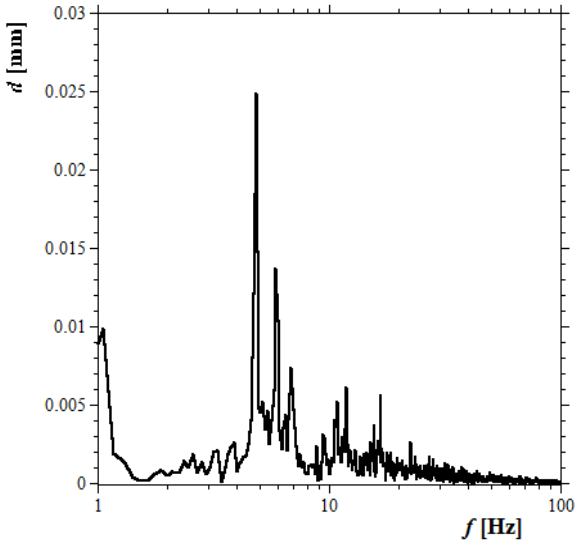

a) F_{PS} = 500 N/m, f_{PWM} = 43 Hz.

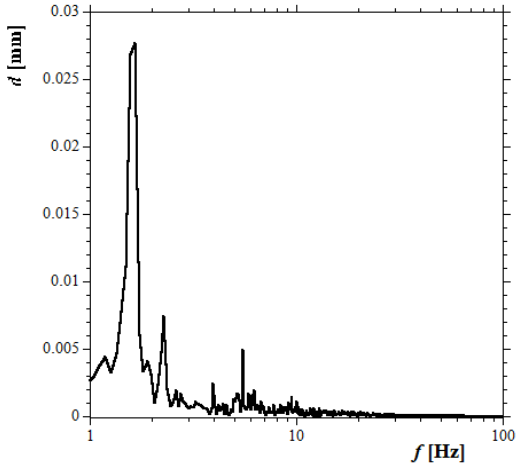

b) F_{PS} = 500 N/m, f_{PWM} = 85 Hz.

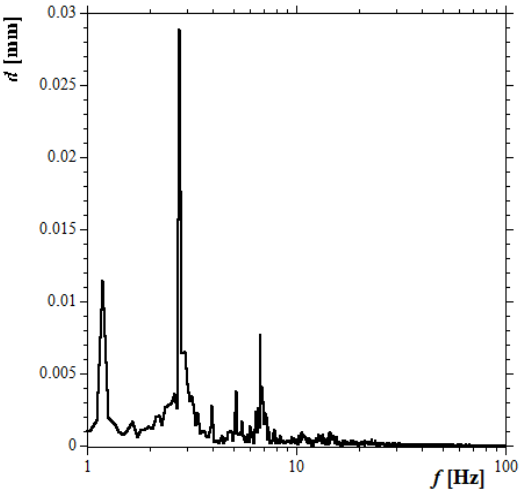

c) F_{PS} = 500 N/m, f_{PWM} = 100 Hz.

Fig. 12 – The frequency spectrum of the output connector displacement.

At this point, a strategy to adjust f_{PWM} for tuning the MSA for optimal magnetostrictive yield seems to consist of the following two steps: (1) find the structural eigenfrequencies, f_m; (2) adjust the PWM frequency, f_{PWM} (f_e) accordingly, aiming for highest displacement and convenient stability, which includes tolerable spurious, secondary oscillations.

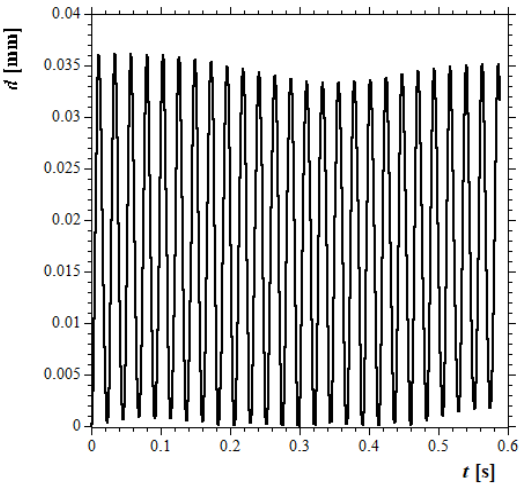

Fig. 13 – The displacement of the output connector for voltage supply, and f_{PWM} = 85 Hz, k = 30 %, F_{PS} = 750 N/m, without friction.

Other factors of concern in this endeavor are the MSA position, frame, and fixing (they may impact the structural modes); the load (here, the MSA produces no external

work); the friction (neglected here), and the thermal stability (neglected here).

A similar discussion may be carried on concerning the other prestress levels and the associated structural eigenfrequencies. Increasing F_{PS} shifts the highest amplitude of the connector's displacement to higher frequencies (from 43 Hz to 47 Hz) to make room to a lower, new, higher frequency (70.51 Hz).

Figure 13 plots the displacement and reveals a very different dynamic for displacement: it carries a lower order frequency envelope signal whose maximum varies in the range 32 μm – 36 μm. Moreover, for higher F_{PS} spurious frequencies are likely to become important. This effect dissipates the work produced by the output connector and reduces the stability of its action.

4. CONCLUSIONS

The mathematical modeling and numerical simulations performed in this study may lead to several conclusions as summarized next.

First, the magnetic field required for the displacement of the MSA connector may be produced with driving and bias coils. The powering scheme utilizes PWM sources, either current or voltage.

The PWM voltage excitation determines a nonlinear variation of inductive nature, which confirms that the PWM voltage excitation represents better the actual operation.

The displacement of the output connector at PWM current excitation is somehow smaller than the displacement when the windings are both PWM voltage excited. It should be noted that the current was deducted from the ampere-turn values computed when the device is powered by a PWM voltage source.

It can be noticed that the displacement in Fig. 6, when the device is powered by a PWM voltage source, stabilizes much faster, respectively after approximately 3 periods. For more realistic results the friction cannot be neglected.

Adding the spring, the prestress, F_{PS}, aims to return the output connector to the initial state (annuls its displacement).

It is important to establish the right level of F_{ps}, and as F_{ps} increases the phase delay between the displacement of the output connector and the coil voltage excitation reduces, according to Fig. 8.

Another effect followed by the increase of the F_{ps}, where the mechanical frequency f_m coincides with the most significant electrical frequency f_e, is the extinguishing of the harmonic components in the displacement of the output connector, but if a certain high F_{ps} value is considered, then the displacement won't pass through zero, so the value of prestress must be chosen accordingly.

Yet another conclusion drawn out of the calculated mechanical eigenfrequencies and by the displacement shape is that at f_{PWM} close to f_m, the harmonics are more prominent. When considering both the functioning at f_{PWM} value, near f_m (Table 1), but also near the fundamental frequency value, which was calculated using the FFT from the exhibited displacement, the output connector is showing a more destabilized behavior.

The spectrum of the PWM signal and that of the MSA structure (for a specific framing and prestress, F_{PS}) are independent quantities that may concur in predicting the MSA functioning. The adjustment of the PWM voltage source frequency, f_{PWM}, should observe the structural eigenfrequencies of the MSA when aiming to enhance the displacement yield of the output connector and a more stable operating mode. Therefore, their knowledge – PWM and structural frequencies – is an initial step in the MSA tuning.

Under load operation mode another type of modeling is, for sure, necessary, but this makes the object of a future research.

ACKNOWLEDGEMENTS

The numerical simulation analysis was conducted in the Laboratory for Multiphysics Modeling, the Faculty of Electrical Engineering, at the University Politehnica of Bucharest.

Received on September 25, 2020

REFERENCES

1. N. Lhermet, F. Claeyssen, H. Fabbro, *Electro-fluidic components based on smart materials for aircraft electro-hydraulic actuators*, Cedrat Technologies, AMA, France, 9th Int. Conf. on New Actuators, ACTUATOR, pp. 718–721, Bremen, Germany, 2004.
2. M. Hemanth, G. S. Mahesh, *Finite element modeling for coupled field analysis of a magnetostrictive material*, Int. J. Eng. Res. & Techn. (IJERT), **2**, *1*, 2013.
3. A. Grunwald, A. G. Olalbi, *Design of a magnetostrictive (MS) actuator*, Sensors and Actuators, **A**, *144*, pp. 161–175, 2008.
4. F. Claeyssen, N. Lhermet, J. Betz, K. Mackay, D. Givord, E. Quandt, H. Kronmuller, *Linear, and rotating magnetostrictive micro-motors*, Proc. Actuator, **98**, Bremen, pp. 375, 1998.
5. E. Quandt, A. Ludwig, *Magnetostrictive actuation in Microsystems*, Sensors, and Actuators, **81**, pp. 275–280, 2000.
6. T. Fukuda, H. Hosokai, H. Ohyama, *Giant Magnetostrictive Alloy (GMA) Applications to Micro Mobile Robot as a Micro Actuator without Power Supply Cables*, Proc. IEEE Micro Electro Mech. Systems, pp. 210–215, 1991.
7. L. Pîslaru-Dănescu, A.M. Morega, M. Morega, *A novel magnetostrictive actuator based on new giant magnetostrictive materials*, IEEE Int. Symp. Adv. Topics El. Eng., Bucharest, 2011.
8. M. Popa, A.M. Morega, L. Pîslaru-Dănescu, M. Morega, *Magnetostrictive actuator – a bi-dimensional analysis*, (in Romanian), Electrical Machines, Materials and Drives, Present and Trends, SME'16, Bucharest, 2016.
9. L. Pîslaru-Dănescu, A.M. Morega, M. Morega, *Electronic drive system of a linear magnetostrictive motor designed for outer space applications*, IEEE Int. Symp. Adv. Topics El. Eng., Bucharest, 2015.
10. M. Popa, A.M. Morega, L. Pîslaru-Dănescu, M. Morega, Y. Veli, *The optimization of the active magnetic material in a magnetostrictive actuator provided with a supplementary electric bias*, (in Romanian) Electrical Machines, Materials, and Drives Present and Trends, SME'18, Bucharest, 2018.
11. A.M.Morega, M. Popa, M. Morega, L. Pîslaru-Dănescu, *Shape and structure optimization of a magnetostrictive cored actuator*, Int. J. Heat Techn., **34**, *1*, pp. S119–S124, 2016.
12. Y. Veli, A.M. Morega, L. Pîslaru-Dănescu, M. Morega, M. Popa, *Study of a linear magnetostrictive motor*, (in Romanian) Electrical Machines, Materials and Drives, Present and Trends SME'19, Bucharest, 2019.
13. U. Ahmed, J. Harju, J. Poutala, P. Ruuskanen, P. Rasilo, R. Kouhia, *Finite Element Method Incorporating Coupled Magneto-Elastic Model for Magneto-Mechanical Energy Harvester*, Conference: Compumag, Daejeon, Korea, June 2017.
14. Z. Deng, M.J. Dapino, *Multiphysics modeling and design of Galfenol-based unimorph harvesters*, Proc. of SPIE, The Int. Soc. for Optical Eng., **9433**, April 2015.
15. B. Rezaeealam, T. Ueno, S. Yamada, *Quasi-static finite element analysis of magnetostrictive vibration energy harvester*, J. Magn. Soc. Japan, **36**, *3*, 2012.
16. J. Slaughter, *Multiphysics models, and magnetostrictive transducer design*, ETERMA Products, Inc., Ames, IA, USA, COMSOL Conference, Boston, USA, 2013.
17. M. Bailoni, Y. Wei, L. Norum, *Mathematical modeling and simulation of magnetostrictive materials by comsol multiphysics*, Proc. COMSOL Conference, Hannover, 2008.
18. J.R. Downing, S.-M. Na, A.B. Flatau, *Compressive prestress effects*

on magnetostrictive behaviors of highly textured Galfenol and Alfenol thin sheets, AIP Advances, **7**, *056420*, 7 pp., 2017.
19. D.C. Jiles, D. L. Atherthon, *Theory of ferromagnetic hysteresis*, J. of Magn. Magn. Mat., **61**, pp. 48–60, 1986.
20. D. C. Jiles, *Theory of magneto-mechanical effect*, J. Phys., D, Appl. Phys., **28**, pp. 1537–1546, 1995.
21. Y. Liu, X.i Gao, C. Chen, *Research of Jiles-Atherton dynamic model in a giant magnetostrictive actuator*, Math. Probl. in Eng., Hindawi Pub. Corp., Article ID 2609069, 2016.
22. F.T. Calkins, *Design, analysis, and modeling of giant magnetostrictive transducers*, Iowa State Univ. Capstones, Theses, and Dissertations, 1997.
23. J.G. Benatar, A.B. Flatau, *FEM implementation of a magnetostrictive transducer*, Smart Struct. Mat.: Smart Struct. Integrated Syst., Ed. A.B. Flatau, Proc. of SPIE, **5764**, pp. 482–493, SPIE, Bellingham, WA, 2005.
24. L. Pîslaru-Dănescu, A.M. Morega, M. Morega, F. Bunea, M. Popa, C.A. Babutanu, *A new type of linear magnetostrictive motor*, El. Eng, **99**, 2, pp. 601-613, 2017.
25. ∴Comsol Multiphysics, V.5.3a, *User's Guide*, 2018.
26. A. Ng., *Control Engineers Guide to Applying Linear Bearings and Guides – The Robot Report*, https://www.therobotreport.com/control-engineers-guide-to-applying-linear-bearings-and-guides/ – accessed in August 2020.
27. ∴ISOTECH, *Slide Bush*, https://www.isotechinc.com/ – accessed in August 2020.